

**High-spin states and lifetimes in  $^{33}\text{S}$  and shell-model interpretation in the  $sd$ - $fp$  space**

S. Aydin,<sup>1,\*</sup> M. Ionescu-Bujor,<sup>2</sup> G. Tz. Gavrilo, <sup>3</sup> B. I. Dimitrov,<sup>3</sup> S. M. Lenzi,<sup>4</sup> F. Recchia,<sup>4</sup> D. Tonev,<sup>3</sup> M. Bouhelal,<sup>5</sup> F. Kavillioglu,<sup>1</sup> P. Pavlov,<sup>3</sup> D. Bazzacco,<sup>4</sup> P. G. Bizzeti,<sup>6</sup> A. M. Bizzeti-Sona,<sup>6</sup> G. de Angelis,<sup>7</sup> I. Deloncle,<sup>8</sup> E. Farnea,<sup>4,†</sup> A. Gadea,<sup>7,9</sup> A. Gottardo,<sup>4,7</sup> N. Goutev,<sup>3</sup> F. Haas,<sup>10</sup> T. Huyuk,<sup>9</sup> H. Laftchiev,<sup>3</sup> S. Lunardi,<sup>4</sup> Tz. K. Marinov,<sup>3</sup> D. Mengoni,<sup>4</sup> R. Menegazzo,<sup>4</sup> C. Michelagnoli,<sup>4</sup> D. R. Napoli,<sup>7</sup> P. Petkov,<sup>3</sup> E. Sahin,<sup>7</sup> P. P. Singh,<sup>11</sup> E. A. Stefanova,<sup>3</sup> C. A. Ur,<sup>4</sup> J. J. Valiente-Dobón,<sup>7</sup> and M. S. Yavahchova<sup>3</sup>

<sup>1</sup>*Department of Physics, Aksaray University, 68100 Aksaray, Turkey*

<sup>2</sup>*Horia Hulubei National Institute of Physics and Nuclear Engineering, Bucharest, Romania*

<sup>3</sup>*Institute for Nuclear Research and Nuclear Energy, BAS, Sofia, Bulgaria*

<sup>4</sup>*Dipartimento di Fisica e Astronomia dell'Università and INFN, I-Sezione di Padova, Padova, Italy*

<sup>5</sup>*Laboratoire de Physique Appliquée et Théorique, Université de Tebessa, Algeria*

<sup>6</sup>*Dipartimento di Fisica dell'Università and INFN Sezione di Firenze, I-Firenze, Italy*

<sup>7</sup>*INFN-Laboratori Nazionali di Legnaro, I-46020 Legnaro, Italy*

<sup>8</sup>*IPNO, IN2P3/CNRS et Université Paris-Sud, F-Orsay, France*

<sup>9</sup>*Instituto de Física Corpuscular, CSIC-Universidad de Valencia, E-Valencia, Spain*

<sup>10</sup>*IPHC, IN2P3/CNRS, Université de Strasbourg, F-Strasbourg, France*

<sup>11</sup>*Department of Physics, Indian Institute of Technology Ropar, Rupnagar-140 001, Punjab, India*

(Received 2 May 2017; revised manuscript received 23 June 2017; published 21 August 2017)

The structure of the  $^{33}\text{S}$  nucleus was investigated in the  $^{24}\text{Mg}(^{14}\text{N},\alpha p)$  fusion-evaporation reaction using a 40-MeV  $^{14}\text{N}$  beam. The level scheme was extended up to an excitation energy of 11.7 MeV and spin  $19/2^+$ . Lifetimes of the intermediate- and high-spin states have been investigated by the Doppler shift attenuation method. Data were compared with different shell-model calculations where effective interactions involving two main shells, the  $sd$  and the  $fp$ , are used.

DOI: [10.1103/PhysRevC.96.024315](https://doi.org/10.1103/PhysRevC.96.024315)

**I. INTRODUCTION**

Nuclei in the  $A \approx 30$ – $40$  mass region are a fundamental testing ground for shell-model calculations. The low-spin positive-parity structure of these nuclei can be reproduced with good accuracy by means of the spherical shell model using the universal  $sd$  interaction (USD) [1,2] or the more recent USDA and USDB [3] interactions. To describe the negative parity states and the high-spin states, one has to consider a larger valence space involving the excitations of one or more particles in the  $fp$  shell. Several different interactions were developed [4–8] and truncated  $sd$ - $fp$  shell-model calculations were performed. The experimental information concerning the level scheme of many nuclei in the region was considerably extended in the last decade by using heavy-ion induced reactions and efficient  $\gamma$  detection systems [9–20]. The data were compared with large shell-model calculations to test the effective interactions proposed for this mass region.

We present here the results of our study of the stable  $^{33}\text{S}$  nucleus by in-beam  $\gamma$ -ray spectroscopy. Experimental data on the level structure of this nucleus is mostly available from  $^{30}\text{Si}(\alpha,n\gamma)^{33}\text{S}$  [21],  $^{32}\text{S}(d,p\gamma)^{33}\text{S}$  [22],  $^{31}\text{P}(^3\text{He},p\gamma)^{33}\text{S}$  [23],  $^{34}\text{P}(^3\text{He},\alpha\gamma)^{33}\text{S}$  [24], and thermal neutron capture [25] reactions. In these studies low- and intermediate-spin states were identified, the highest spins being  $9/2^+$  and  $11/2^-$  for the 4049- and 4867-keV levels of positive and negative parity, re-

spectively. Lifetimes were determined for states up to 5.3 MeV in  $^{30}\text{Si}(\alpha,n\gamma)$  and  $^{32}\text{S}(d,p\gamma)$  reactions by the Doppler-shift attenuation method (DSAM) [21,26,27]. Recently, two studies were reported in which the  $^{33}\text{S}$  nucleus was populated by heavy-ion fusion-evaporation reactions and the  $\gamma$  rays were detected by high-efficiency arrays. Bisoi *et al.* [28] used the  $^{27}\text{Al}(^{12}\text{C},\alpha pn)$  reaction and included two states at 7180- and 7819-keV excitation energy, assigned as  $11/2^+$  and  $15/2^-$ , respectively. They performed also lifetime measurements by DSAM with the aim to investigate the evolution of the collectivity with spin. Very recently Fu *et al.* [29] populated  $^{33}\text{S}$  in the  $^{26}\text{Mg}(^{13}\text{C},2n\alpha)$  reaction and identified five more excited states, however, without spin and parity assignments. In the present study the level scheme of  $^{33}\text{S}$  was extended up to the  $19/2^+$  level at 11700 keV. Spins and parities were assigned to the new states and to the recently reported states [28,29] and lifetime measurements have been performed. The new experimental results are presented in Sec. II and compared with detailed theoretical shell-model calculations in Sec. III. Conclusions are given in Sec. IV. Preliminary results of this work were previously communicated in [30,31].

**II. EXPERIMENTAL PROCEDURE AND RESULTS**

High-spin states of  $^{33}\text{S}$  have been populated via the fusion-evaporation reaction  $^{24}\text{Mg}(^{14}\text{N},\alpha p)^{33}\text{S}$  using a 40-MeV  $^{14}\text{N}$  beam delivered by the LNL XTU-Tandem accelerator. The target consisted of 99.7% isotopically enriched  $^{24}\text{Mg}$ , 1-mg/cm<sup>2</sup> thick, evaporated on an 8-mg/cm<sup>2</sup> gold layer. The  $\gamma$  rays were detected using the  $4\pi$ -GASP array [32] composed of 40 Compton-suppressed large volume high-purity Ge detectors

\*01sezgin@gmail.com

†Deceased.

positioned in seven rings at the angles of  $34^\circ$ ,  $60^\circ$ ,  $72^\circ$ ,  $90^\circ$ ,  $108^\circ$ ,  $120^\circ$ , and  $146^\circ$  with respect to the beam axis. Events were collected when at least two germanium detectors fired in coincidence. The data were sorted into a symmetric  $\gamma - \gamma$  matrix and seven asymmetric matrices having the detectors in each ring on the first axis, and all detectors on the second axis. Energy and efficiency calibrations were performed with a standard  $\gamma$ -ray source of  $^{152}\text{Eu}$ .

### A. Level scheme

The level scheme of  $^{33}\text{S}$  was constructed on the basis of coincidence relationships in spectra created with appropriate

gates on the symmetric  $\gamma - \gamma$  matrix. A few  $\gamma$  transitions, de-exciting the highest-lying states, were totally Doppler shifted and were studied in spectra registered by the detectors placed at  $90^\circ$ . Multipolarities of the transitions were deduced based on angular distribution ratios  $R_{\text{ADO}}$  defined as:  $R_{\text{ADO}} = (I_\gamma(34^\circ) + I_\gamma(146^\circ))/2I_\gamma(90^\circ)$ , where  $I_\gamma(\theta)$  are the efficiency-corrected  $\gamma$ -ray intensities from spectra gated on the axis with all the detectors. Because of the presence of Doppler-broadened shapes, the  $\gamma$  intensities were obtained by integrating on the broadened lines. In the present experimental conditions typical  $R_{\text{ADO}}$  values are  $\approx 0.75$  for pure dipole stretched transitions, and  $\approx 1.35$  for quadrupole stretched transitions and for transitions with  $\Delta J = 0$ . In the case of

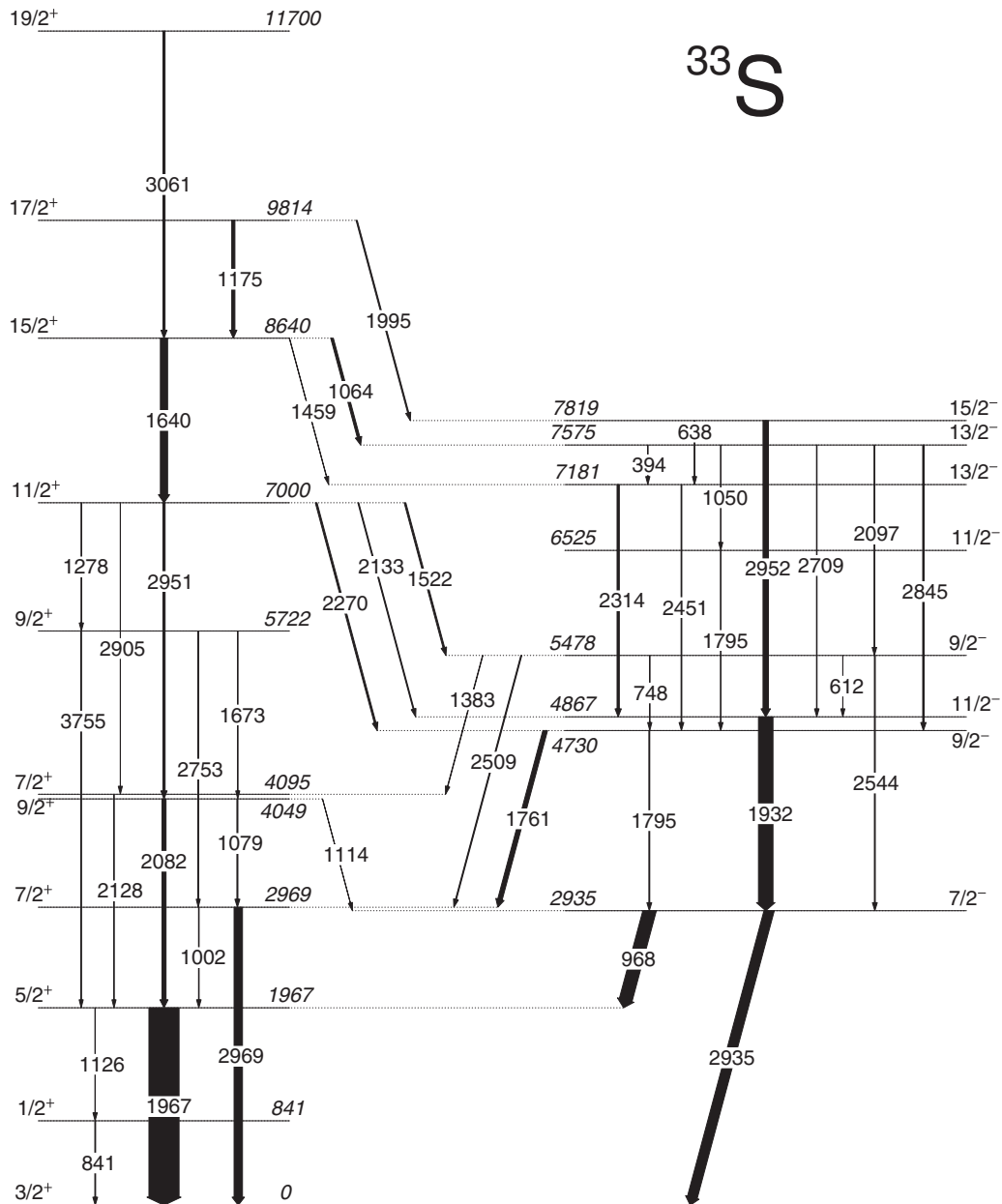


FIG. 1. Level scheme of  $^{33}\text{S}$  established in the present work. The transitions between states of the same parity are shown as vertical arrows, while the transitions connecting states of different parities are shown as tilted arrows. The widths of the arrows correspond to the relative intensities of the observed  $\gamma$ -ray transitions.

TABLE I. Initial state energies, spins, and parities for initial and final states and transition energies in  $^{33}\text{S}$ , as well as  $R_{\text{ADO}}$ , relative intensities, multipolarities, and  $\delta$  mixing ratios. The states up to the excitation energy of 4867 keV were observed in light-ion induced reactions [34]. The newly included states and transitions are marked with a star (\*). The states and transitions reported recently [29] without spin-parity and multipolarity assignment, are marked by two stars (\*\*).

$E_i$ (keV)	$J_i^\pi$	$J_f^\pi$	$E_\gamma$ (keV)	$R_{\text{ADO}}$	$I_\gamma^{\text{rel}}$	Multipolarity ( $\delta$ )
841.0(2)	$1/2^+$	$3/2^+$	841.0(2)		27(1)	$M1 + E2 (+0.18(5))^a$
1967.2(3)	$5/2^+$	$1/2^+$	1126.2(2)	1.35(4)	12(2)	$E2$
		$3/2^+$	1967.2(3)	0.46(5)	1000(57)	$M1 + E2 (-0.60(12))^a$
2934.7(4)	$7/2^-$	$5/2^+$	967.5(3)	0.74(2)	434(15)	$E1$
		$3/2^+$	2934.7(4)	1.17(4)	331(13)	$M2 + E3 (-0.32(17))^a$
2969.2(14)	$7/2^+$	$5/2^+$	1002.3(8)	0.74(5)	19(2)	$M1$
		$3/2^+$	2969.2(14)	1.29(5)	279(23)	$E2$
4048.6(6)	$9/2^+$	$7/2^+$	1079.2(7)	0.48(8)	33(8)	$M1 + E2 (-0.33(4))^a$
		$7/2^-$	1113.8(14)	0.75(4)	6(2)	$E1$
		$5/2^+$	2081.5(6)	1.27(6)	135(14)	$E2$
4095.1(14)	$7/2^+$	$5/2^+$	2127.7(14)	0.95(11)	3(1)	$M1 + E2 (+0.19(2))^a$
4730.1(9)	$9/2^-$	$7/2^+$	1760.8(9)	0.79(4)	151(20)	$E1$
		$7/2^-$	1795.4(13)	1.45(7)	29(4)	$M1 + E2 (+1.0(3))^a$
4866.7(6)	$11/2^-$	$7/2^-$	1931.9(6)	1.20(9)	482(28)	$E2$
5478(1)**	$9/2^-$	$11/2^-$	611.7(4)*	0.81(10)	3(1)	$M1$
		$9/2^-$	748.3(5)*	1.35(12)	6(2)	$M1$
		$7/2^+$	1383.3(7)**	0.73(6)	15(4)	$E1$
		$7/2^+$	2509.2(7)**	0.79(9)	32(7)	$E1$
		$7/2^-$	2543.7(6)**	1.37(8)	30(7)	$M1 + E2 (+0.7(3))$
5722(2)*	$9/2^+$	$9/2^+$	1673.1(13)*		0.9(3)	
		$7/2^+$	2752.5(14)*		1.5(5)	
		$5/2^+$	3754.5(25)*	1.36(11)	2.1(8)	$E2$
6525(2)*	$11/2^-$	$9/2^-$	1795.0(20)*	0.44(10)	20(7)	$M1 + E2 (-0.5(2))$
7000(1)**	$11/2^+$	$9/2^+$	1278.2(9)*	0.47(10)	9(3)	$M1 + E2 (-0.5(2))$
		$9/2^-$	1521.5(6)**	0.75(6)	53(9)	$E1$
		$11/2^-$	2133.2(6)**	1.31(9)	30(6)	$E1$
		$9/2^-$	2269.8(5)**	0.75(5)	56(9)	$E1$
		$7/2^+$	2905.1(3)**		4(1)	
		$9/2^+$	2951.3(8)**	0.84(3)	73(12)	$M1$
7181(2) <sup>b</sup>	$13/2^-$	$11/2^-$	2314.3(20)	1.31(8)	75(9)	$M1 + E2 (+0.4(1))$
		$9/2^-$	2450.9(25)	1.34(13)	25(4)	$E2$
7575(1)*	$13/2^-$	$13/2^-$	394.4(5)*	1.34(10)	5(1)	$M1$
		$11/2^-$	1050.3(9)*	0.69(10)	6(2)	$M1$
		$9/2^-$	2097.0(15)*	1.27(7)	17(5)	$E2$
		$11/2^-$	2708.7(15)*	0.71(8)	17(5)	$M1$
		$9/2^-$	2845.3(17)**	1.37(5)	47(12)	$E2$
7819(1)	$15/2^-$	$13/2^-$	637.9(10)*	0.82(10)	4(1)	$M1$
		$11/2^-$	2952.2(12)	1.38(10)	179(32)	$E2$
8640(1)**	$15/2^+$	$13/2^-$	1064.1(11)**	0.73(5)	85(18)	$E1$
		$13/2^-$	1458.5(10)*		6(2)	
		$11/2^+$	1639.6(9)**	1.37(7)	239(37)	$E2$
9814(2)**	$17/2^+$	$15/2^+$	1174.5(17)**	0.77(4)	105(29)	$M1$
		$15/2^-$	1995.1(19)*	0.75(11)	37(14)	$E1$
11700(2)*	$19/2^+$	$15/2^+$	3060.8(18)*	1.33(11)	69(28)	$E2$

<sup>a</sup>Ref. [34].

<sup>b</sup>State previously known [28], spin-parity changed in this work.

mixed multipolarities,  $R_{\text{ADO}}$  depends on the value and sign of the mixing coefficient  $\delta$  (see below).

The established level scheme of  $^{33}\text{S}$  is shown in Fig. 1. The energies, spins, and parities of the levels, as well as the transition energies, the ADO ratios, the relative intensities, and the multipolarities are given in Table I. Figure 2 illustrates coincidence spectra registered by the detectors at  $90^\circ$  obtained

by gating on the  $\gamma$  rays of 968, 2935, and 2969 keV which are depopulating the low-lying states in  $^{33}\text{S}$ , as well as on the 1064-keV transition de-exciting a higher-lying level.

In a recent study Bisoi *et al.* [28] reported three transitions de-exciting the states at 7180 and 7819 keV assigned as  $11/2^+$  and  $15/2^+$ , respectively. Very recently Fu *et al.* [29]

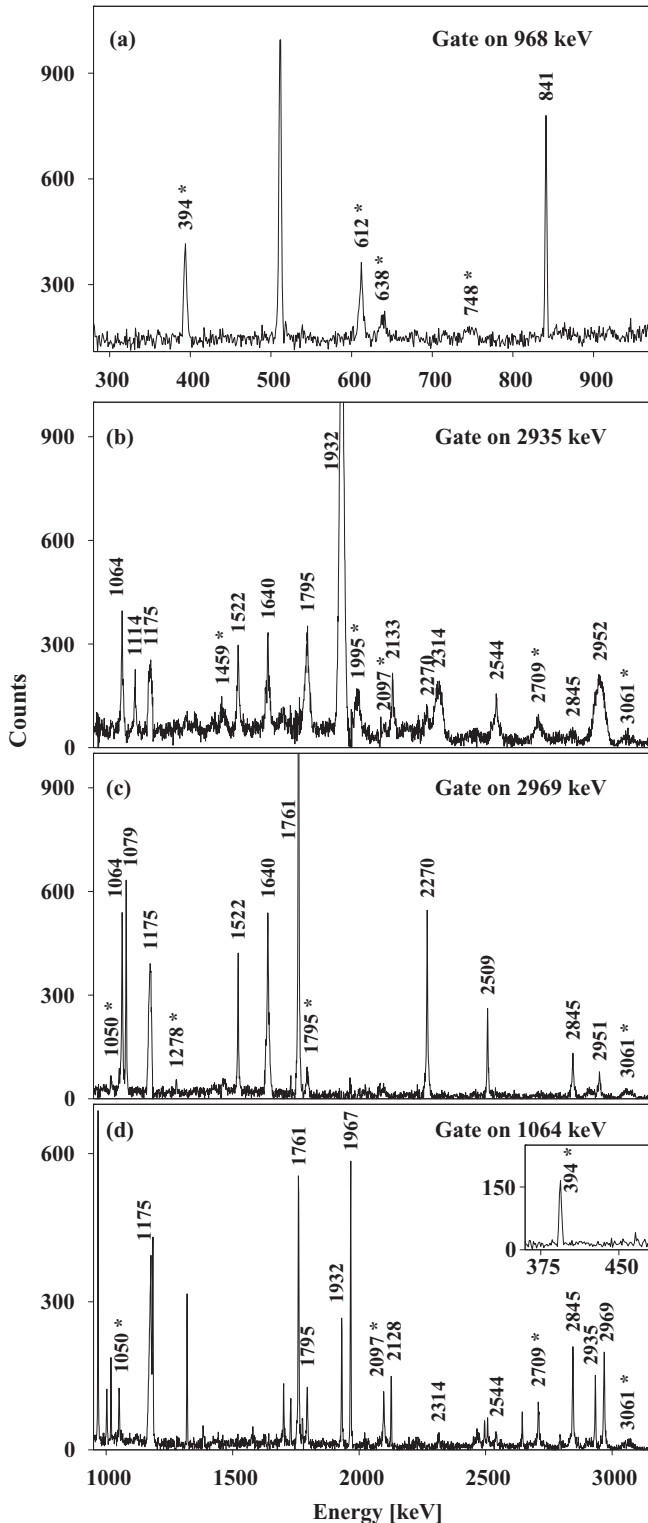


FIG. 2. Background-subtracted coincidence spectra registered by the detectors at  $90^\circ$ , obtained from the asymmetric  $\gamma - \gamma$  matrix with gates on  $\gamma$ -ray transitions of (a) 968, (b) 2935, (c) 2969, and (d) 1064 keV on the axis with all the detectors. The new transitions are marked with a star (\*).

reported 12 transitions in  $^{33}\text{S}$  but without determining their multiplicities. The presence of the transitions reported in the above mentioned studies was confirmed by our data. In

some cases, however, there are differences, up to 1.5 keV, between the energies inferred in our work and the previously reported values. In addition we found 15 new transitions and identified four new states (as seen in Table I). Spins and parities of the new states and of the states previously reported in [28,29] have been assigned on the basis of multiplicities of their de-exciting transitions deduced from the  $R_{\text{ADO}}$  values. Most transitions were assigned of the pure dipole or quadrupole type (Table I). A few transitions were found as having a mixed dipole+quadrupole character. In view of the short lifetimes of the investigated states (see next subsection) all quadrupole transitions were assigned as  $E2$ , as a  $M2$  multipolarity would correspond to transition strengths much higher than the upper limit of 3 W.u. recommended for this mass region [33]. The same argument was applied in the case of mixed dipole+quadrupole transitions, that were taken as  $M1 + E2$ .  $R_{\text{ADO}}$  have been calculated for these transitions using various mixing ratio  $\delta$  values, and have been compared with the experimental  $R_{\text{ADO}}$  values. On the basis of the agreement between the experimental and the corresponding calculated  $R_{\text{ADO}}$ ,  $\delta$  values have been assigned to the mixed dipole+quadrupole transitions. As in our earlier work [11], values of the alignment parameter  $\sigma/J$  slightly decreasing with spin, from  $\approx 1$  at low spins to  $\approx 0.7$  at high spins, were used in the calculations.

The previously known yrast negative-parity states  $7/2^-$ ,  $9/2^-$ , and  $11/2^-$  at energies of 2935, 4730, and 4867 keV, respectively, were populated in our experiment and the measured  $R_{\text{ADO}}$  values for the de-exciting transitions confirmed the assigned multiplicities. The 2952-keV transition assigned as de-exciting the state at 7819 keV in Ref. [28] was well populated [see Fig. 2(b)] and its  $E2$  multipolarity was confirmed. This gives support for the  $15/2^-$  assignment for the 7819-keV state. Our data revealed that this level is de-excited also by a new transition of 638 keV [see Fig. 2(a)] feeding the state at 7181 keV reported as  $11/2^+$  in Ref. [28]. On the basis of the  $R_{\text{ADO}}$  value of the 638-keV transition we assigned to it a dipole character, and therefore changed the spin of the 7181-keV state to  $13/2$ . A negative parity was assigned based on the quadrupole character of the 2451-keV de-exciting transition feeding the first  $9/2^-$  state. The 7181-keV state was therefore identified as the yrast  $13/2^-$  level. The  $R_{\text{ADO}}$  value of 1.31(8) derived for the 2314-keV transition to the yrast  $11/2^-$  state was reproduced by calculations with a mixing coefficient  $\delta = +0.4(1)$ .

The level at 5478-keV excitation energy was assigned as the second  $9/2^-$  state. This state was reported by Fu *et al.* [29] to decay by three transitions of 1384, 2511, and 2545 keV. We confirmed these transitions and we included two new transitions, of 612 and 748 keV [see Fig. 2(a)] feeding the yrast  $11/2^-$  and  $9/2^-$  states, respectively. The spin and parity were assigned based on the dipole character of the 612-keV transition and the mixed  $M1 + E2$  multipolarity derived for the 2544-keV transition to the yrast  $7/2^-$  state. The assignment is confirmed by the  $E1$  multipolarity of the 2509- and 1383-keV transitions populating the known  $7/2^+$  states at 2969- and 4095-keV excitation energy.

Our data revealed the presence of a new transition of 1795 keV in coincidence with the known  $\gamma$  rays of 1761,

1795, and 2969 keV [see Fig. 2(c)]. This transition was placed in the level scheme to decay from a new state at 6525 keV to the  $9/2^-$  state at 4730 keV. The  $R_{\text{ADO}}$  value of 0.44(10) (Table I) pointed to a mixed  $M1 + E2$  multipolarity for the 1795-keV transition, therefore spin-parity  $11/2^-$  were assigned to the new state. On the basis of the agreement between experimental and calculated  $R_{\text{ADO}}$ , a mixing coefficient  $\delta = -0.5(2)$  was given to the new 1795-keV transition.

A new state identified at 7575 keV was found to decay via five transitions of 394, 1050, 2097, 2709, and 2845 keV to the lower-lying negative parity states. This state was assigned as the second  $13/2^-$  state, based on the  $E2$  multipolarity of the 2845- and 2097-keV transitions to the yrast and yrare  $9/2^-$  states, respectively. Moreover the spin and parity assignment is supported by the measured  $R_{\text{ADO}}$  values of the 394- and 2709-keV transitions to the yrast  $13/2^-$  and  $11/2^-$  states.

On the positive-parity side, a new state was found at 5722 keV de-excited by the weak 1673-, 2753-, and 3755-keV transitions to the lower-lying positive-parity states. The 3755-keV transition feeding the yrast  $5/2^+$  state was established as  $E2$  on the basis of the measured  $R_{\text{ADO}}$ , leading to  $J^\pi = 9/2^+$  for the 5722-keV state. A state placed at 7000-keV excitation energy was reported by Fu *et al.* [29] to decay by five transitions of 1520, 2133, 2270, 2951, and 2905 keV. These transitions were also seen in our data. Moreover we found a new transition of 1278 keV, populating the 5722-keV  $9/2^+$  state. The  $R_{\text{ADO}}$  value of 0.47(10) for this transition (Table I) indicated a mixed  $M1 + E2$  multipolarity and it was reproduced by the calculations for  $\delta = -0.5(2)$ . Therefore we assigned the state at 7000 keV as the yrast  $11/2^+$  level. The assignment is supported by the  $R_{\text{ADO}}$  values of the other de-exciting transitions, as seen in Table I. The 2952-keV transition feeding the  $9/2^+$  4049-keV state was assigned

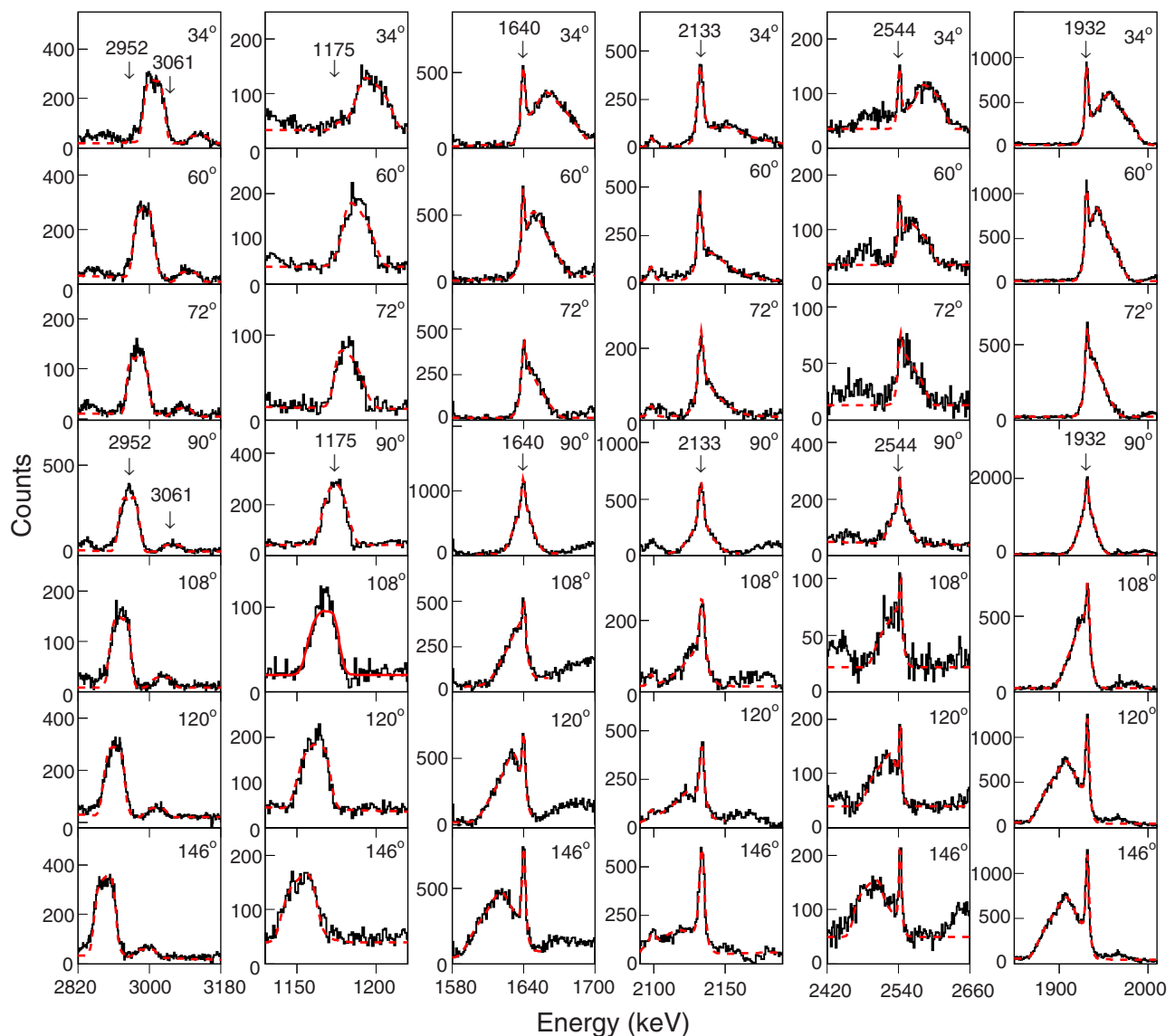


FIG. 3. Experimental and calculated lineshapes for transitions in  $^{33}\text{S}$ . The coincidence spectra were created with narrow gates on lower-lying transitions emitted from stopped nuclei. The fitted DSAM spectra are shown in red dashed lines.

TABLE II. Lifetimes determined in the present work for excited states in  $^{33}\text{S}$ . Values derived previously by Carr *et al.* [21] and Bisoi *et al.* [28] are also presented.

$E_x$ (keV)	$J^\pi$	$\tau$ (ps)		
		Ref. [21]	Ref. [28]	Present work
4730.1	$9/2^-$	0.082(22)	0.19(4)	0.13(4)
4866.7	$11/2^-$	0.36(9)	0.30(5)	0.40(10)
5478.4	$9/2^-$	—	—	$\leq 0.04$
6525.1	$11/2^-$	—	—	0.18(5)
6999.9	$11/2^+$	—	—	0.32(6)
7181.0	$13/2^-$	—	$< 0.08$	0.09(3)
7575.4	$13/2^-$	—	—	$\leq 0.04$
7818.9	$15/2^-$	—	$< 0.02$	0.08(3)
8639.5	$15/2^+$	—	—	0.41(4)
9814.0	$17/2^+$	—	—	0.17(4)
11700.3	$19/2^+$	—	—	0.05(2)

as  $M1$ , while the 1522-, 2133-, and 2270-keV transitions populating the 5478-, 4867-, and 4730-keV negative-parity states, respectively, were assigned as  $E1$ .

In the work of Fu *et al.* [29] a state at 8641-keV excitation energy was included, de-excited by the 1641-keV transition to the 7000-keV level. We observed an intense transition of 1640 keV in coincidence with all  $\gamma$  rays from the  $11/2^+$  7000-keV state. On the basis of the assigned  $E2$  multipolarity for the 1640-keV transition, we identified the 8640-keV state as the yrast  $15/2^+$  state. In the level scheme proposed in Ref. [29] this level is also de-excited by a 2848-keV transition feeding a state at 5793 keV that decays by a transition of 1063 keV. However, this placement was not confirmed by our data. We found a 1064-keV transition in coincidence with the 394-, 1050-, 2097-, 2709-, and 2845-keV transitions de-exciting the  $13/2^-$  state at 7575 keV, as well as with the transitions depopulating the lower-lying negative parity states [Fig. 2(d)]. Therefore the 1064-keV transition was placed between the  $15/2^+$  state and the second  $13/2^-$  state. Its measured  $R_{\text{ADO}}$  multipolarity supports the  $E1$  assignment. Our data revealed also a new weak transition of 1459 keV placed between the 8640-keV state and the yrast  $13/2^-$  state at 7181 keV. The highest spin populated in our experiment is  $19/2^+$  assigned to the new state at 11 700 keV. This level decays by the  $E2$  3061-keV transition to the  $15/2^+$  state.

### B. Lifetime measurements

The data of the present experiment have been analyzed to obtain lifetime information by applying the Doppler shift attenuation method. From the asymmetric  $\gamma$ - $\gamma$  matrices spectra have been created with narrow gates on the low-lying transitions of 968 and 2935 keV, emitted from stopped nuclei. In these spectra all transitions de-exciting the intermediate- and high-spin states exhibited lineshapes. The analysis was performed using the LINESHAPE computer code [35]. The slowing down history of  $^{33}\text{S}$  recoils in the target and backing was simulated using Monte Carlo techniques and a statistical distribution was created for the projection of the recoil velocity with respect to the direction of the detected  $\gamma$  ray. The code

was modified to include, at each level, side populations from two independent levels. For the description of the electronic and nuclear scattering the Ziegler stopping powers [36,37] have been adopted.

The lineshape analysis started with the transitions from the highest levels in  $^{33}\text{S}$  and continued with the lower lying transitions. The obtained information for the higher levels was used in the analysis of the lower states. At each level the intensity balance of feeding and decaying transitions was calculated using the  $\gamma$  intensities of Table I, allowing one to establish the amount of the fast side-feeding from unobserved transitions. Examples of experimental lineshapes and the corresponding fits are illustrated in Fig. 3. From the present DSAM analysis lifetime values or upper limits were inferred for all intermediate- and high-spin states investigated in the present work, excepting the very weakly populated  $9/2^+$  state at 5722 keV. The results are collected in Table II. Assigned errors include an additional systematic uncertainty of 10% from the stopping power calculation. The lifetimes measured previously by Carr *et al.* [21] using the  $^{30}\text{Si}(\alpha, n\gamma)^{33}\text{S}$  reaction and by Bisoi *et al.* [28] in heavy-ion induced reaction are also given in the table. The presently determined lifetimes for the

EXP.	USD	PSDPF	sdfp
	$17/2^+$ 13784		
		$17/2^+$ 13042	
			$19/2^+$ 12441
$19/2^+$ 11700	$15/2^+$ 11415		
		$15/2^+$ 10959	
			$17/2^+$ 10126
$17/2^+$ 9814	$13/2^+$ 9275		
		$13/2^+$ 8880	
$15/2^+$ 8640			$15/2^+$ 8898
			$13/2^+$ 8739
			$9/2^+$ 8520
			$9/2^+$ 8158
			$11/2^+$ 7364
$11/2^+$ 7000	$11/2^+$ 6732	$11/2^+$ 6634	$7/2^+$ 6680
$9/2^+$ 5722	$9/2^+$ 5966	$9/2^+$ 5778	
			$7/2^+$ 4351
$7/2^+$ 4095	$9/2^+$ 4243	$9/2^+$ 4111	
$9/2^+$ 4049	$7/2^+$ 3973	$7/2^+$ 4019	
$7/2^+$ 2969	$7/2^+$ 2891	$7/2^+$ 3096	$5/2^+$ 3233
$5/2^+$ 1967	$5/2^+$ 1895	$5/2^+$ 1897	
$1/2^+$ 841	$1/2^+$ 779	$1/2^+$ 809	
$3/2^+$ 0	$3/2^+$ 0	$3/2^+$ 0	$3/2^+$ 0

FIG. 4. Comparison between experimental positive parity states in  $^{33}\text{S}$  and shell-model calculated states using different model spaces and interactions. In the figure is not included the  $19/2^+$  state calculated using the USD and PSDPF interactions, predicted at 17 224- and 16 784-keV excitation energy, respectively.

yrast  $9/2^-$  and  $11/2^-$  states are closer to those derived by Carr *et al.* [21]. Note also that the lifetimes derived for the yrast  $13/2^-$  and  $15/2^-$  states do not support the upper limits established for these states by Bisoi *et al.* [28].

### III. DISCUSSION

To interpret the observed properties in  $^{33}\text{S}$ , detailed shell-model calculations for both excitation energies and  $\gamma$  transition probabilities have been performed. A first calculation (USD) was performed with the code ANTOINE [38] in the  $sd$  shell-model space using the USD residual interaction [2]. The comparison between the experimental positive-parity levels and the calculated ones is illustrated in Fig. 4. We note the good agreement between experimental and calculated states up to the spin  $11/2^+$ . On the other hand the high-spin states are predicted too high in energy. This indicates that at high spins the  $sd$  shell-model space is not enough for a good description of the states and that intruder excitations into the  $fp$  shell have to be considered.

The experimental results obtained in  $^{33}\text{S}$  have been also compared with  $p-sd-pf$  calculations, which use the PSDPF interaction [8] to describe both  $0\hbar\omega$  positive-parity states and  $1\hbar\omega$  negative-parity intruder states. As shown in Fig. 4, the results for the positive parity states are similar to those obtained with the USD interaction. A good description is provided up to the  $11/2^+$  state. In addition, the negative parity states are remarkably well described by the PSDPF calculations, as illustrated in Fig. 5. The calculations give the correct ordering of all levels, excepting the second  $13/2^-$  state that is predicted above the  $15/2^-$  in contrast with the

EXP.	PSDPF	sdfp
		$13/2^-$ — 10683
		$15/2^-$ — 9720
		$13/2^-$ — 8745
$15/2^-$ — 7819	$13/2^-$ — 7716	$11/2^-$ — 7658
$13/2^-$ — 7575	$15/2^-$ — 7646	$9/2^-$ — 6866
$13/2^-$ — 7181		$9/2^-$ — 5863
$11/2^-$ — 6525	$13/2^-$ — 6752	$11/2^-$ — 5442
	$11/2^-$ — 6418	
$9/2^-$ — 5478	$9/2^-$ — 5214	
$11/2^-$ — 4867	$11/2^-$ — 4851	
$9/2^-$ — 4730	$9/2^-$ — 4837	
		$7/2^-$ — 2644
$7/2^-$ — 2935	$7/2^-$ — 2853	
$3/2^+$ — 0	$3/2^+$ — 0	$3/2^+$ — 0

FIG. 5. Comparison between negative parity experimental and shell-model predicted levels in  $^{33}\text{S}$ .

experiment. Moreover the excitation energies of all levels are well reproduced. This indicates that up to spin  $15/2^-$  the structure of the negative parity states involves only one excitation in the  $fp$  orbitals.

We have also performed calculations using the  $sdfp$  effective interaction [6], in a truncated space that assumes a  $^{28}\text{Si}$  inert core. The model space involves the  $s_{1/2}$ ,  $d_{3/2}$ ,  $f_{7/2}$ , and  $p_{3/2}$  orbitals, while no excitations from the  $d_{5/2}$  orbit are considered. As shown in Fig. 4 the energies of the positive parity low-spin states are overpredicted by these calculations. Moreover the ordering of the levels is not correct, with the  $9/2^+$  states calculated above the  $11/2^+$  state. The same behavior is observed for the negative parity states (see Fig. 5) where the calculated energies, except for the  $7/2^-$  state, are higher than the experimental values. It is obvious that the closure of the  $d_{5/2}$  orbit has a strong impact on the structure of these states. On the other hand the results compare relatively well with data for the high-spin positive parity states. Note that the yrast  $13/2^+$  state is calculated very close to the  $15/2^+$  state. The  $13/2^+$  state might therefore be weakly populated as the

TABLE III. Experimental positive-parity level energies in  $^{33}\text{S}$  (from present work) and  $^{35}\text{S}$  (from Ref. [19]) compared with calculated values using the  $sdfp$  interaction. For each state are given the occupation numbers in the  $fp$  shell for neutrons ( $\nu fp$ ) and for protons ( $\pi fp$ ).

$J^\pi$	$E_x^{\text{exp}}(\text{MeV})$	$E_x^{\text{calc}}(\text{MeV})$	$\nu fp$	$\pi fp$
$^{33}\text{S}$				
$3/2_1^+$	0.00	0.00	0.11	0.11
$1/2_1^+$	0.84			
$5/2_1^+$	1.97	3.23	0.15	0.14
$7/2_1^+$	2.97	4.35	0.15	0.10
$9/2_1^+$	4.05	8.16	0.85	0.47
$7/2_2^+$	4.10	6.68	1.46	0.48
$9/2_2^+$	5.72	8.52	0.81	0.51
$11/2_1^+$	7.00	7.36	1.67	0.58
$13/2_1^+$	—	8.74	1.17	0.99
$15/2_1^+$	8.64	8.90	1.69	0.62
$17/2_1^+$	9.81	10.13	1.18	1.02
$19/2_1^+$	11.70	12.44	1.28	0.81
$^{35}\text{S}$				
$3/2_1^+$	0.00	0.00	0.42	0.12
$1/2_1^+$	1.57	2.00	0.88	0.18
$5/2_1^+$	2.72	3.36	0.87	0.17
$7/2_1^+$	3.59	3.70	1.88	0.15
$5/2_2^+$	3.89	4.54	1.77	0.15
$9/2_1^+$	4.82	5.45	2.04	0.18
$9/2_2^+$	4.90	5.83	2.04	0.18
$9/2_3^+$	5.41	6.60	2.10	0.19
$11/2_1^+$	5.88	4.73	2.03	0.18
$11/2_2^+$	6.30	6.57	2.09	0.42
$13/2_1^+$	—	6.16	2.01	0.23
$15/2_1^+$	7.18	5.87	1.90	0.67
$17/2_1^+$	8.02	8.57	1.86	0.52

feeding from the higher-spin states is mostly directed toward the  $15/2^+$  state. This is in accordance with the fact the  $13/2^+$  state is not observed experimentally.

To have a deeper insight on the calculations we have extracted the occupation numbers of protons and neutrons in the  $f_{7/2}p_{3/2}$  orbits. The results for the positive parity states are summarized in the upper part of Table III. The contribution of nucleon excitation to the  $fp$  shell is very small for low-spin states, but becomes important for the high-spin states. An important outcome of the calculations is that the promotion to the  $fp$  shell of a proton-neutron pair is favored compared to the promotion of a pair of protons or neutrons. This type of coupling was observed also in the high-spin structure of  $^{34}\text{S}$  [10] and  $^{31}\text{P}$  [11].

In a recent study [19] we have established the level scheme up to spins  $17/2^+$  and  $13/2^-$  in the neighboring odd-mass  $^{35}\text{S}$  nucleus. Similar to the  $^{33}\text{S}$  nucleus, the negative-parity states have been described well with the PSDPF calculations, while the high-spin positive parity states were described by the  $sdfp$  calculations. In the lower part of Table III we present for comparison the results for the occupation numbers of protons and neutrons in the  $f_{7/2}p_{3/2}$  orbits in the  $^{35}\text{S}$  nucleus. As seen

in the table, the structure of the high-spin states in this nucleus is dominated by the excitation of a pair of two neutrons, with only small mixing of a proton-neutron pair excitation. These results reveal a change in the intrinsic structure of high-spin positive parity states in the neighboring  $^{33}\text{S}$  and  $^{35}\text{S}$  nuclei. This can be understood in the  $sdfp$  calculation because of the reduced number of valence nucleons in  $^{33}\text{S}$  with respect to  $^{35}\text{S}$ . From shell model wave functions it results that for the  $13/2^+$  and  $17/2^+$  states, the excitation of a proton and a neutron to the  $fp$  orbits is largely dominant. The probability of exciting a  $pn$  pair coupled to  $J = 7, T = 0$  is maximum for the  $17/2^+$  state. For the other signature ( $11/2^+$ ,  $15/2^+$ , and  $19/2^+$ ), a more mixed configuration is obtained.

The experimental reduced transition probabilities for transitions with different multiplicities in  $^{33}\text{S}$  have been calculated using the measured half-lives (from Ref. [34] and this work) and the branching ratios (BR) derived in most cases from the presently determined  $\gamma$ -ray intensities. In the case of transitions with mixed multiplicities, the  $\delta$  mixing ratios given in Table I were used. The results for the  $B(M1)$  and  $B(E2)$  reduced transition probabilities are compared in Table IV with the USD, PSDPF, and  $sdfp$  shell-model

TABLE IV. Experimental reduced transition probabilities  $B(M1)$  and  $B(E2)$  in  $^{33}\text{S}$  compared to shell-model calculations.

$E_{\text{lev}}^{\text{exp}}$ (keV)	$T_{1/2}^{\text{exp}}$ (ps)	$J_i^{\pi}$	$J_f^{\pi}$	$E_{\gamma}^{\text{exp}}$ (keV)	BR <sup>b</sup> (%)	$B(M1)(\times 10^{-3}\mu_N^2)$				$B(E2)(e^2\text{fm}^4)$			
						exp	USD	PSDPF	$sdfp$	exp	USD	PSDPF	$sdfp$
841.0	1.15(12) <sup>a</sup>	$1/2_1^+$	$3/2_1^+$	841.0	100	56(7)	30	33		37(24)	18	17	
1967.2	0.094(14) <sup>a</sup>	$5/2_1^+$	$1/2_1^+$	1126.2	1.2(2)					40(9)	18	25	
			$3/2_1^+$	1967.2	99(6)	40(7)	8	13	7	53(20)	52	52	20
2969.2	0.059(8) <sup>a</sup>	$7/2_1^+$	$5/2_1^+$	1002.3	6.4(4)	42(7)	36	50	144				
			$3/2_1^+$	2969.2	94(8)					39(6)	30	32	21
4048.6	0.212(53) <sup>a</sup>	$9/2_1^+$	$7/2_1^+$	1079.2	19(1)	25(8)	4	1	85	34(14)	32	31	0.12
			$5/2_1^+$	2081.5	78(4)					53(18)	48	55	12
4095.1	0.031(8) <sup>a</sup>	$7/2_2^+$	$5/2_1^+$	2127.7	100	128(34)	174	160	2	14(5)	26	25	2
6999.9	0.222(42) <sup>b</sup>	$11/2_1^+$	$9/2_2^+$	1278.2	4(1)	3(1)	48	52	173	6(4)	23	28	0.09
			$9/2_1^+$	2951.3	32(6)	2(1)	272	302	37				
			$7/2_2^+$	2905.1	1.8(5)					0.22(7)	22	17	49
8639.5	0.284(28) <sup>b</sup>	$15/2_1^+$	$11/2_1^+$	1639.6	73(14)					122(26)	37	38	57
9814.0	0.118(28) <sup>b</sup>	$17/2_1^+$	$15/2_1^+$	1174.5	74(30)	152(72)	196	192	357				
11700.3	0.035(14) <sup>b</sup>	$19/2_1^+$	$15/2_1^+$	3060.8	100					60(24)	9	13	28
4730.1	0.090(28) <sup>b</sup>	$9/2_1^-$	$7/2_1^-$	1795.4	16(3)	6(3)		10	4	27(12)		45	4
4866.7	0.277(69) <sup>b</sup>	$11/2_1^-$	$7/2_1^-$	1931.9	100					76(19)		53	39
5478.4	$\leq 0.03^b$	$9/2_2^-$	$11/2_1^-$	611.7	3.9(4)	$\geq 224$		63	633				
			$9/2_1^-$	748.3	6.7(4)	$\geq 210$		383	468				
			$7/2_1^-$	2543.7	35(2)	$\geq 19$		9	54	$\geq 21$		37	7
6525.1	0.125(35) <sup>b</sup>	$11/2_2^-$	$9/2_1^-$	1795.0	100	44(14)		14	38	49(32)		71	7
7181.0	0.062(21) <sup>b</sup>	$13/2_1^-$	$11/2_1^-$	2314.3	75(12)	33(13)		31	8	14(9)		61	0.13
			$9/2_1^-$	2450.9	25(5)					26(10)		23	29
7575.4	$\leq 0.03^b$	$13/2_2^-$	$13/2_1^-$	394.4	5.4(14)	$\geq 1156$		41	3				
			$11/2_2^-$	1050.3	6.1(6)	$\geq 74$		1	0				
			$9/2_2^-$	2097.0	18(6)					$\geq 83$		6	15
			$11/2_1^-$	2708.7	18(6)	$\geq 12$		1	7				
			$9/2_1^-$	2845.3	51(15)					$\geq 51$		8	2
7818.9	0.055(21) <sup>b</sup>	$15/2_1^-$	$13/2_1^-$	637.9	2(1)	55(34)		148	519				
			$11/2_1^-$	2952.2	98(24)					45(20)		63	35

<sup>a</sup>Reference [34].

<sup>b</sup>Present study.

TABLE V. Experimental reduced transition probabilities  $B(E1)$ ,  $B(M2)$ , and  $B(E3)$  in  $^{33}\text{S}$  compared to shell-model calculations using the PSDPF residual interaction.

$E_{\text{lev}}^{\text{exp}}$ (keV)	$T_{1/2}^{\text{exp}}$ (ps)	$J_i^\pi$	$J_f^\pi$	$E_\gamma^{\text{exp}}$ (keV)	$BR^b$ (%)	$B(E1)(\times 10^{-5} e^2 \text{fm}^2)$		$B(M2)(\mu_N^2 \text{fm}^2)$		$B(E3)(e^2 \text{fm}^6)$	
						exp	PSDPF	exp	PSDPF	exp	PSDPF
2934.7	28.2(1.4) <sup>a</sup>	$7/2_1^-$	$5/2_1^+$	967.5	57(3)	1.0(1)	4.8	3.28(17)	8.20	926(48)	179
			$3/2_1^+$	2934.7	43(3)						
3220.7	0.027(5) <sup>a</sup>	$3/2_1^-$	$5/2_2^+$	353.0	.4(1) <sup>a</sup>	147(46)	95				
			$3/2_2^+$	907.3	.4(1) <sup>a</sup>	9(3)	3				
			$5/2_1^+$	1253.6	.3(1) <sup>a</sup>	2(1)	13				
			$1/2_1^+$	2379.6	60(3) <sup>a</sup>	72(14)	248				
			$3/2_1^+$	3220.7	39(3) <sup>a</sup>	19(4)	31				
4730.1	0.09(3) <sup>a</sup>	$9/2_1^-$	$7/2_1^+$	1760.8	84(14)	75(28)	511				
5478.4	$\leq 0.03^b$	$9/2_2^-$	$7/2_2^+$	1383.3	17(5)	$\geq 93$	160				
			$7/2_1^+$	2509.2	37(9)	$\geq 34$	720				

<sup>a</sup>Reference [34].<sup>b</sup>Present study.

calculations. The measured reduced transition probabilities for parity changing  $E1$ ,  $M2$ , and  $E3$  transitions de-exciting the lowest-lying negative-parity states in  $^{33}\text{S}$  are given in Table V together with the estimates of the calculations with the PSDPF residual interaction. In the USD and *sdfp* calculations free nucleon  $g$  factors have been used for deriving the  $B(M1)$  values, while the  $B(E2)$  have been obtained using for the effective electric charges  $e_v^{\text{eff}} = 0.5e$  and  $e_\pi^{\text{eff}} = 1.5e$ . The PSDPF calculations were performed with parameters fitted using USDA and USDB through new experimental values given in Ref. [39]. The values  $g_{vs}^{\text{eff}} = -3.55$ ,  $g_{vl}^{\text{eff}} = -0.09$ ,  $g_{\pi s}^{\text{eff}} = 5.150$ ,  $g_{\pi l}^{\text{eff}} = 1.159$ , were adopted for the  $B(M1)$  and  $B(M2)$  calculations. The neutron and proton effective charges were  $(-0.485, 0.515)$ ,  $(0.45, 1.36)$ , and  $(0.48, 1.36)$  for the  $B(E1)$ ,  $B(E2)$ , and  $B(E3)$  estimations, respectively.

We note an overall agreement between the experimental and calculated reduced transition probabilities. As seen in Table IV, in the case of positive-parity states with  $J^\pi \leq 9/2^+$  most experimental reduced transition probabilities are very well reproduced by the USD and PSDPF calculations, providing evidence in favor of the reliability of the calculated wave functions. The  $B(E2)$  values for the transitions de-exciting the  $15/2^+$  and  $19/2^+$  states are underestimated in all calculations, the predictions being, however, better in the *sdfp* calculations in which the involved states are described by the promotion of two nucleons into the  $fp$  shell. On the negative parity side both PSDPF and *sdfp* calculations are in satisfactory agreement with the experimental data. Note that large discrepancies were observed in all calculations for the transitions de-exciting the yrast  $11/2^+$  state and the second  $13/2^-$  state. This could indicate that the structure of these states is more complex, involving both significant excitations from the  $d_{5/2}$  orbital, not considered in the *sdfp* calculations, and multiple particle-hole excitations to the  $fp$  orbitals, not taken into account in the PSDPF calculations.

In their recent study of  $^{33}\text{S}$ , Biso *et al.* [28] performed lifetime measurements and reported  $B(E2)$  values of 16(3) and  $>28$  W.u. for the 1932- and 2952-keV transitions de-exciting the  $11/2^-$  and  $15/2^-$  states, respectively. Based on the large

$B(E2)$  of the 2952-keV transition they suggested an increase in collectivity with spin along the negative-parity sequence, that may evolve to a superdeformed rotational band. Such a feature was, however, not confirmed in the present work. The  $B(E2)$  deduced for the 1932- and 2952-keV transitions by using the measured lifetimes (Table II) were found constant within errors, with values of 12(3) and 7(3) W.u., respectively. A similar behavior was observed also for the positive parity levels, with  $B(E2)$  values of 8(3), 19(4), and 10(4) W.u. for the 2082-, 1640- and 3061-keV transitions de-exciting the yrast  $9/2^+$ ,  $15/2^+$ , and  $19/2^+$  states, respectively.

#### IV. CONCLUSIONS

The nucleus  $^{33}\text{S}$  was studied in its high-spin region using the  $^{24}\text{Mg}(^{14}\text{N}, \alpha p)$  fusion-evaporation reaction. The high sensitivity of the experimental setup allowed us to extend the level scheme by adding 15 new transitions and four new levels. Spins and parities of the new states and of five previously reported states have been assigned. Using the DSAM, the lifetimes of 11 states have been determined. The data were compared to large scale shell-model calculations performed with the code ANTOINE using the USD, PSDPF, and *sdfp* effective interactions. The positive-parity states up to spin  $11/2^+$  and all negative-parity states up to spin  $15/2^-$  have been well described by using the PSDPF interaction. Calculations using the *sdfp* interaction revealed that excitations involving the promotion of a proton-neutron pair to the  $fp$  shell play an important role in the structure of the positive-parity high-spin states of  $^{33}\text{S}$ .

#### ACKNOWLEDGMENTS

Authors are thankful to the XTU Tandem staff of Laboratori Nazionali di Legnaro for the good quality delivered beam. This research was supported by Bulgarian Science Fund under Contract No. DN08/6 and by the program for support of young scientists, Bulgarian Academy of Sciences under Contract No. DFNP 48.

- [1] B. H. Wildenthal, *Prog. Part. Nucl. Phys.* **11**, 5 (1984).
- [2] B. A. Brown and B. H. Wildenthal, *Annu. Rev. Nucl. Part. Sci.* **38**, 29 (1988).
- [3] B. A. Brown and W. A. Richter, *Phys. Rev. C* **74**, 034315 (2006).
- [4] E. K. Warburton, J. A. Becker, and B. A. Brown, *Phys. Rev. C* **41**, 1147 (1990).
- [5] Y. Utsuno, T. Otsuka, T. Mizusaki, and M. Honma, *Phys. Rev. C* **60**, 054315 (1999).
- [6] E. Caurier, K. Langanke, G. Martinez-Pinedo, F. Nowacki, and P. Vogel, *Phys. Lett. B* **522**, 240 (2001).
- [7] E. Caurier, F. Nowacki, and A. Poves, *Phys. Rev. Lett.* **95**, 042502 (2005).
- [8] M. Bouhelal, F. Haas, E. Caurier, F. Nowacki, and A. Bouldjedri, *Nucl. Phys. A* **864**, 113 (2011).
- [9] C. E. Svensson *et al.*, *Phys. Rev. Lett.* **85**, 2693 (2000).
- [10] P. Mason *et al.*, *Phys. Rev. C* **71**, 014316 (2005).
- [11] M. Ionescu-Bujor *et al.*, *Phys. Rev. C* **73**, 024310 (2006).
- [12] F. Della Vedova *et al.*, *Phys. Rev. C* **75**, 034317 (2007).
- [13] R. Kshetri *et al.*, *Nucl. Phys. A* **781**, 277 (2007).
- [14] M. Ionescu-Bujor *et al.*, *Phys. Rev. C* **80**, 034314 (2009).
- [15] R. Chakrabarti *et al.*, *Phys. Rev. C* **84**, 054325 (2011).
- [16] P. C. Bender *et al.*, *Phys. Rev. C* **85**, 044305 (2012).
- [17] S. Aydin *et al.*, *Phys. Rev. C* **86**, 024320 (2012).
- [18] A. Bisoi *et al.*, *Phys. Rev. C* **89**, 024303 (2014).
- [19] S. Aydin *et al.*, *Phys. Rev. C* **89**, 014310 (2014).
- [20] S. S. Bhattacharjee *et al.*, *Phys. Rev. C* **91**, 044306 (2015).
- [21] P. E. Carr, D. C. Bailey, J. L. Durell, L. L. Green, A. N. James, J. F. Sharpey-Schafer, and D. A. Viggars, *J. Phys. A* **6**, 685 (1973).
- [22] J. A. Becker, L. F. Chase, Jr., D. B. Fossan, and R. E. McDonald, *Phys. Rev.* **146**, 761 (1966).
- [23] K. T. Knöpfle, M. Rogge, C. Mayer-Böricke, D. S. Gemmell, L. Meyer-Schützmeister, H. Ohnuma, and N. G. Puttaswamy, *Phys. Rev. C* **4**, 818 (1971).
- [24] J. Dubois, *Nucl. Phys. A* **117**, 533 (1968).
- [25] S. Raman, R. F. Carlton, J. C. Wells, E. T. Jurney, and J. E. Lynn, *Phys. Rev. C* **32**, 18 (1985).
- [26] F. Brandolini and C. Signorini, *Phys. Lett. B* **30**, 342 (1969).
- [27] G. van Middelkoop and G. A. P. Engelbertink, *Nucl. Phys. A* **138**, 601 (1969).
- [28] A. Bisoi *et al.*, *Phys. Rev. C* **90**, 024328 (2014).
- [29] B. Fu *et al.*, *Phys. Rev. C* **94**, 034318 (2016).
- [30] G. Tz. Gavrilov *et al.*, *J. Phys.: Conf. Ser.* **533**, 012050 (2014).
- [31] B. I. Dimitrov *et al.*, *J. Phys.: Conf. Ser.* **533**, 012049 (2014).
- [32] C. Rossi Alvarez, *Nucl. Phys.* **3**, 10 (1993).
- [33] P. M. Endt, *At. Data Nucl. Data Tables* **23**, 3 (1979).
- [34] J. Chen and B. Singh, *Nucl. Data Sheets* **112**, 1393 (2011).
- [35] J. C. Wells and N. R. Johnson, in Report No. ORNL-6689 (Oak Ridge National Laboratory, 1991), p. 44.
- [36] J. F. Ziegler, *The Stopping and Range of Ions in Matter*, Vols. 3 and 5 (Pergamon Press, Oxford, 1980).
- [37] J. F. Ziegler, J. P. Biersack, and V. Littmark, *The Stopping Power and Range of Ions in Solid*, Vol. 1 (Pergamon Press, Oxford, 1985).
- [38] E. Caurier and F. Nowacki, *Acta Phys. Pol. B* **30**, 705 (1999).
- [39] W. A. Richter, S. Mkhize, and B. A. Brown, *Phys. Rev. C* **78**, 064302 (2008).